Research Repository UCD

Title	Threshold virtual impedance current limiting design for grid-forming converters considering voltage vector location
Authors(s)	Zhao, Xianxian, Kestelyn, Xavier, Flynn, Damian
Publication date	2023-11-16
Publication information	Zhao, Xianxian, Xavier Kestelyn, and Damian Flynn. "Threshold Virtual Impedance Current Limiting Design for Grid-Forming Converters Considering Voltage Vector Location." Institution of Engineering and Technology, November 16, 2023. https://doi.org/10.1049/icp.2023.3219.
Conference details	Renewable Power Generation and Future Power Systems Conference 2023 (RPG 2023 UK), Glasgow, United Kingdom, 15-16 November 2023
Publisher	Institution of Engineering and Technology
Item record/more information	http://hdl.handle.net/10197/26568
Publisher's statement	This paper is a postprint of a paper submitted to and accepted for publication in Renewable Power Generation and Future Power Systems Conference 2023 (RPG 2023 UK) and is subject to Institution of Engineering and Technology Copyright. The copy of record is available at the IET Digital Library.
Publisher's version (DOI)	10.1049/icp.2023.3219

Downloaded 2026-05-01 23:34:49

The UCD community has made this article openly available. Please share how this access benefits you. Your story matters! (@ucd_oa)

© Some rights reserved. For more information

Threshold Virtual Impedance Current Limiting Design for Grid-Forming Converters Considering Voltage Vector Location

Xianxian Zhao[1*], Xavier Kestelyn[2], Damian Flynn[1]

[1]School of Electrical and Electronic Engineering, University College Dublin, Belfield, Dublin, Ireland
[2]ULR 2697–L2EP, Centrale Lille, Junia ISEN Lille, Arts et Metiers Institute of Technology, University of Lille, France
**xianxian.zhao@ucd.ie*

Keywords: Grid-forming converter, threshold virtual impedance current limiter, current saturation control, transient / synchronisation stability.

Abstract

Threshold virtual impedance (TVI) is a promising current limiting technology to ensure the hardware integrity of grid-forming converters (GFMs), as it maintains the voltage source characteristic behind an impedance. Existing TVI parameter design principles are based on limiting the GFM current to a maximum value when a bolted fault is applied at the point of common coupling (PCC). However, adopting existing TVI parameter design practices can cause the GFM current to exceed the maximum value after a fault is cleared, or under a large grid phase jump, since the angular difference between the GFM internal and PCC voltage vector can be large, causing the voltage across the virtual impedance and output transformer to exceed that assumed for TVI parameter design. Hence, the worst case design scenario is not during a fault, but during the subsequent recovery period, or under a large phase jump. Here, a new TVI parameter design process is proposed based on the GFM internal voltage vector being in anti-phase to the PCC voltage vector. However, the new approach should not be applied directly as the GFM current capacity may not be fully used. Hence, three alternative strategies are proposed, with a combined approach being recommended based on electromagnetic transient (EMT) simulations for a range of case studies.

1 Introduction

With the increasing integration of renewable energy sources, high-voltage long-distance transmission, DC grids, and power electronic (PE) converter-interfaced loads, very high PE shares are anticipated in future power systems [1]. Existing converters are mostly controlled as "grid-following", using a phase-locked loop (PLL) to synchronise the voltage angle and frequency at the connection point, in order to precisely follow the active and reactive power setpoints [2]. Since synchronisation to the grid voltage is required for grid-following converters (GFL), as part of ensuring stable outputs, it follows that when the GFL share reaches a certain threshold that synchronisation can no longer be ensured [3, 4].

Consequently, the concept of "grid-forming" is proposed, with the key difference being that grid-forming converters (GFMs) independently create their own internal voltage angle and frequency without relying on a PLL, by, for example, using an independent external power reference incorporating power feedback. One of the simplest GFM concepts mimics an ideal AC voltage source, by fixing their frequency at the rated value. Thus, GFMs can maintain their voltage angle and provide an immediate response to voltage and frequency disturbances, providing similar capabilities to synchronous generators, such as an inertial response, blackstart capability and forming a voltage reference for GFLs. Consequently, GFMs are often seen as a replacement for synchronous generators in future power grids.

Due to the fast controllability of voltage source converters, GFMs without current limiting can tightly control the grid voltage, with reduced transient stability concerns against large disturbances, assuming robust small-signal stability. However, given that voltage source converters (VSCs) have much lower overcurrent ability compared to synchronous generators (typically, a VSC can only cope with double its rated current for ≈1 ms [5]), current limiting control is necessary to protect the converters, which greatly impacts on GFM controllability, and, hence, system transient stability.

Current limiting control techniques for GFMs can be categorised as current reference saturation, virtual impedance, and a combination of both. Saturation techniques can be implemented in different ways [6], such as d-axis or q-axis current reference priority, or scaling the d- and q-axis current references simultaneously. Such methods can strictly limit the GFM current, but the outer voltage control loop becomes inactive, and the GFM operates as a current source rather than as a voltage source [6, 7]. Combining the inner current saturation limitation and outer power reference adjustment is proposed in [8], but it is unclear if the method is applicable in practice, since the power reference adjustment depends on the GFM output voltage, but the latter is influenced by the former. Threshold virtual impedance (TVI) current limiting emulates the effect of an impedance when the converter current exceeds a defined value [9]. Therefore, GFM voltage source behaviour is retained, but behind a larger impedance.

Standard principles for calculating the TVI parameter are based on limiting the GFM current to a maximum value, I_{max}, when a bolted fault is applied at the point of common coupling (PCC) [9-12]. However, the GFM current could still exceed I_{max} after a fault is cleared, as the angular difference between the GFM internal voltage and the PCC voltage vector needs to be considered. In other words, the worst case

scenario is not during a fault, but during the post-fault period, or following a large phase jump. Hence, a new TVI parameter design is proposed based on the GFM internal voltage vector being in anti-phase to the PCC voltage vector. However, since a larger TVI impedance will mean that the GFM current capacity may not be fully used, three strategies are proposed, i.e. enhancing GFM transient stability; switching between "old" and "new" TVI parameter design approaches; and, combining "old" TVI with a scaling-based current saturation control. The remainder of the paper is organised as follows: Section 2 introduces classical droop control based GFM, Section 3 describes existing TVI parameter design principles, while Section 4 proposes a modified TVI design process, and three strategies are studied to limit the GFM current, as well as maximise utilisation of GFM capacity. Finally, Section 5 concludes the paper.

2 Classical Droop Based Grid-Forming Converter

Grid-forming converters are designed to act as voltage sources instead of current sources (which is the case for grid-following inverters), and, therefore, they have the potential to replace synchronous machines (which create the voltage in today's power systems). The structure of a droop control based GFM, as studied here, are shown in Fig. 1, representing the classical structure seen in [7, 13]. The GFM consists of a DC/AC converter (here, the DC voltage source and DC/AC converter are assumed ideal) and a transformer and RLC filter, while the control hierarchy consists of P/f voltage angle control, outer output voltage amplitude V_o control loop (including Q/V droop control, threshold virtual impedance current limiting control and damping enhancement), inner cascaded voltage and current control loops. In the following, essential equations relevant to the presented studies are described, with vector quantities indicated in bold.

For classical droop control, equations for active power and frequency, P/f, droop control are given as (1)-(4), which model the converter active power injection, measurement and filtering of the active power input, P/f droop control, and the converter internal voltage angle.

$$P = v_{od} i_{od} + v_{oq} i_{oq}, \tag{1}$$

$$\frac{dp_m}{dt} + \omega_c p_m = \omega_c P, \tag{2}$$

$$\omega_{vsm} = \omega_0 + m_p (P_{ref} - p_m), \tag{3}$$

$$\frac{1}{\omega_b}\frac{d\theta_{vsm}}{dt} = \omega_{vsm}. \tag{4}$$

The equations for the d- and q-axis output voltage references are given as (5), where Δe_d and Δe_q are the d- and q-axis voltage generated by damping enhancement control, while $m_q \Delta Q$ is the voltage drop due to reactive power and voltage amplitude droop control (Q/V). Equations (6)-(8) represent the TVI control, while (9) calculates the converter current.

$$v_{od}^* = V_{ref} + m_q \Delta Q - \Delta e_d - \Delta v_{VId}, \tag{5a}$$

$$v_{oq}^* = 0 - \Delta e_q - \Delta v_{VIq}, \tag{5b}$$

$$\Delta v_{VId} = R_{VI} i_{cd} - X_{VI} i_{cq}, \tag{6a}$$

$$\Delta v_{VIq} = R_{VI} i_{cq} + X_{VI} i_{cd}, \tag{6b}$$

$$R_{VI} = k_{pR}^{VI} \max(0, i_c - I_{nom}), \tag{7}$$

$$X_{VI} = \sigma_{X/R}^{VI} R_{VI}, \tag{8}$$

$$i_c = \sqrt{i_{cd}^2 + i_{cq}^2}. \tag{9}$$

Due to the fast switching characteristics of voltage source converters, the voltage and current references are perfectly followed. With this assumption, the $L_f C_f$ filter and the inner voltage and current control can be simplified as a voltage source, $v_{od}^* + j v_{oq}^*$, where v_{od}^* and v_{oq}^* are expressed as (5a) and (5b). Fig. 1 can then be re-drawn as Fig. 2 in a static *abc* reference frame, where the impacts of Q/V droop control and damping enhancement are ignored, as they are much smaller in magnitude than TVI control, due to the small coefficients and the inclusion of high-pass filters.

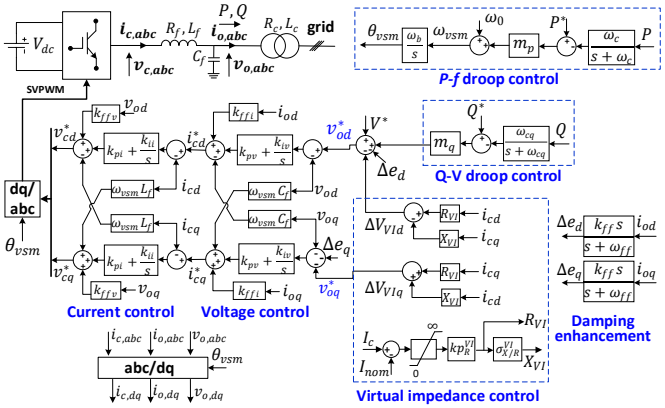

Fig. 1 Droop control-based GFM with a LCL filter, with the TVI current limiting control included in the outer output voltage amplitude control loop.

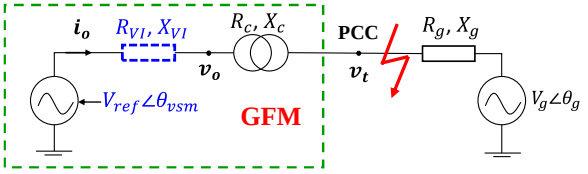

Fig. 2 Equivalent circuit of GFM of Fig. 1 under TVI current limiting control, connecting to an equivalent AC grid.

3 Existing TVI Parameter Design Principles

3.1 Existing TVI Parameters Design Principles

The design principles of existing TVI schemes limit the GFM current to I_{max} when a bolted fault is applied at the PCC [10, 11]. Consequently, the virtual resistance proportional gain k_{pR}^{VI} in (8) is calculated using (8-11) by assuming $\boldsymbol{i_c} = \boldsymbol{i_o}$, as the LCL filter can be simplified by ignoring the capacitor [8].

$$I_{max} = \frac{V_{ref}}{\sqrt{(R_c + R_{VI}^{max})^2 + (X_c + X_{VI}^{max})^2}}, \tag{10}$$

$$R_{VI}^{max} = k_{pR}^{VI}(I_{max} - I_{nom}), \tag{11}$$

where, X_{VI}^{max} is expressed in the same form as (8), based on the virtual inductance resistance ratio $\sigma_{X/R}^{VI}$ given beforehand, in order to satisfy transient stability and current damping characteristics [10], while R_c and X_c are the resistance and reactance of the output transformer, as seen in Fig. 1.

3.2 Limitations of Existing TVI Parameter Design

For the conventional TVI parameter design of (10), the worst case scenario, i.e. maximum voltage amplitude across the virtual impedance and output transformer, would be V_{ref}, during a fault. This assumption is generally true, since both the angle between the GFM internal voltage, $V_{ref}\angle\theta_{vsm}$, and the PCC voltage, $\boldsymbol{v_t}$, and the amplitude, V_t, are small, Fig. 2. However, post-fault, or for a large phase-jump, the maximum voltage amplitude can reach $V_{ref} + V_t$, as seen from Fig. 3.

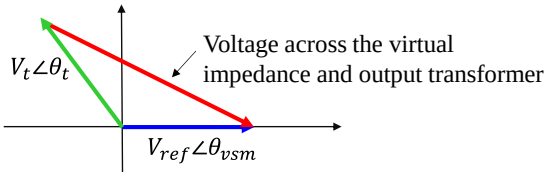

Fig. 3 Voltage vector relationship for the circuit of Fig. 2.

As the PCC voltage $\boldsymbol{v_t}$ is a dependent variable, the equivalent AC voltage $\boldsymbol{v_g}$ can be used instead. Hence the maximum voltage amplitude becomes $V_{ref} + V_g$. Once the TVI parameter is set based on (10), the GFM maximum current is then fixed, which is decided by the transmission line and virtual impedance, and the GFM voltage setpoint V_{ref} and grid voltage V_g, and is irrelevant to fault duration and the GFM active power setpoint, as can be seen in Fig. 2.

To demonstrate the above analysis, Cases 1-4 are simulated on a simple test system under bolted faults and phase jumps. Note that all simulations are performed using Modelica [14], as implemented using Dymola software, whereby all modelling details are completely transparent and user-created models can be easily integrated. A variable integration time step is applied, with an integration tolerance of 0.0001.

Case 1: The GFM in Fig. 1 under the existing TVI parameter design of (10) is connected to an equivalent AC grid with an equivalent resistance and reactance R_g and X_g of 0.02 pu and 0.2 pu (based on converter capacity base) and $V_g = 1$ pu, as seen in Fig. 2. The GFM active and reactive power, and voltage setpoints, are given as $P_{ref} = 0.9$ pu, $Q_{ref} = 0$ pu, and $V_{ref} = 1$ pu. TVI parameters of $\sigma_{X/R}^{VI} = 2.5$ and $k_{pR}^{VI} = 1.2825$ are obtained using (10), where the maximum current limit, I_{max}, for calculating k_{pR}^{VI}, is 1.2 pu. Other GFM parameters are shown in Table 1, where the inner voltage and current proportional-integral controller parameters are taken from [15]. A bolted 3-phase fault is applied at 2 s at the PCC, and cleared after 100, 150, 200, 250 or 300 ms.

Case 2: Same as Case 1, but the active power setpoint P_{ref} is varied from 0.7 to 0.95 pu. The fault duration is 250 ms.

Case 3: Same as Case 1, but the post-fault transmission line reactance X_g is varied, i.e. 0.02, 0.2 or 0.8 pu. The fault duration is 250 ms, and, as shown in Fig. 4, it is cleared by disconnecting the second line.

Case 4: Same as Case 1, but a phase jump (-30°, -40°, -50°, -60°) disturbance is now applied to the AC grid.

The simulation results for Case 1 are shown in Fig. 5, which indicates that the GFM current is limited at 1.2 pu during the fault, Fig. 5(a). However, when the fault is cleared, the current exceeds the maximum limit for all considered fault durations, except the 100 ms fault. For the longer faults, Fig. 5(b) shows that the active power output actually turns negative, before recovering to its pre-fault state, which illustrates that the angle between the GFM internal voltage and the grid voltage varies from <180° to >180°. In Fig. 5(c) the PCC voltage initially reduces before recovering to the pre-fault value, due to the voltage drop across the virtual impedance (which increases with the GFM current). Although different fault durations are considered, the peak current, lowest active power and lowest PCC voltage are consistent (i.e. 1.34 pu, -1.1 pu and 0.74 pu, respectively). For the 100 ms fault, the GFM current remains below 1.2 pu once the fault is cleared, while the active power output and PCC voltage directly recover to their pre-fault values, unlike what happens for longer faults, since the angle between the GFM internal voltage and PCC voltage is comparatively small when the fault is cleared.

The GFM current profiles for Case 2 are shown in Fig. 6, where it is seen that the maximum current, lowest active power and PCC voltage are the same as those in Case 1, despite variations in the active power setpoint. The GFM current profiles for Case 3, with the grid impedance being changed, are shown in Fig. 7. It is seen, not surprisingly, that the maximum post-fault current reduces with an increasing grid impedance. Finally, the impact of phase jumps in Case 4 are shown in Fig. 8, with similar behaviour observed for small and large phase jumps as that for short and long duration faults in Fig. 5. Again the maximum GFM current for different phase jumps is comparable to that seen in Case 1, with the post-fault dynamics also looking similar.

In conclusion, Cases 1-4 demonstrate that

- For the existing TVI parameter design of (10), the GFM current is not limited to I_{max}, from which it follows that the PCC voltage falling to zero does not represent the worst case scenario for determining the TVI parameters.
- The maximum GFM current under TVI current limiting control does not depend on fault duration, phase jump angle or active power setpoint, but is affected by the connecting transmission line impedance.

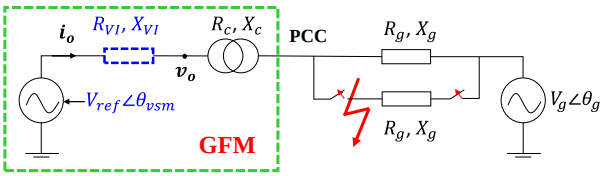

Fig. 4 Three-phase fault applied at PCC for Case 3, with the fault cleared by disconnecting the second line.

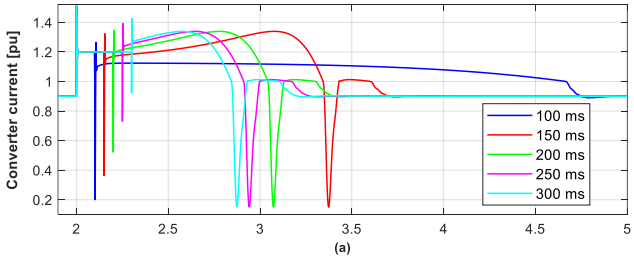

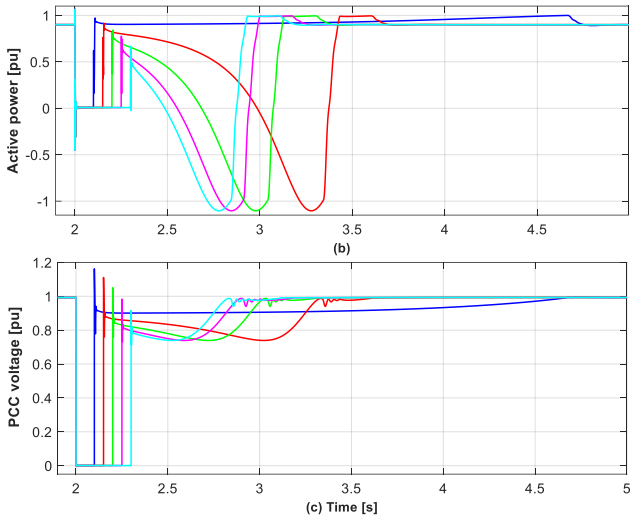

Fig. 5 GFM operation under Case 1 for various 3-phase faults (a) converter current, (b) active power, and (c) PCC voltage.

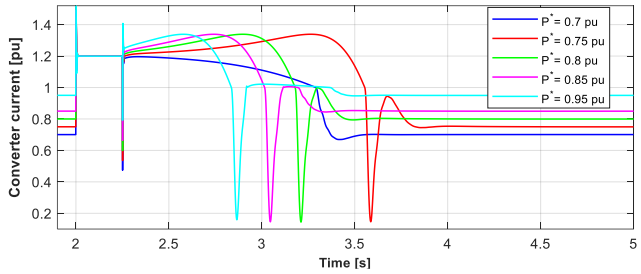

Fig. 6 GFM converter current under Case 2 for different GFM active power setpoints.

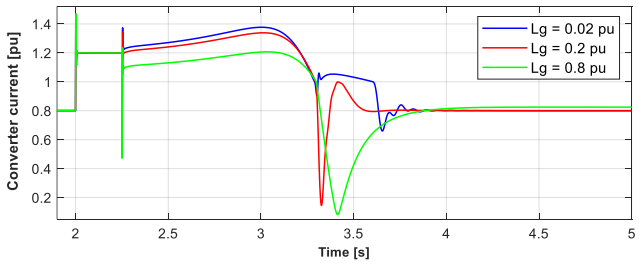

Fig. 7 GFM converter current under Case 3 for different transmission line lengths.

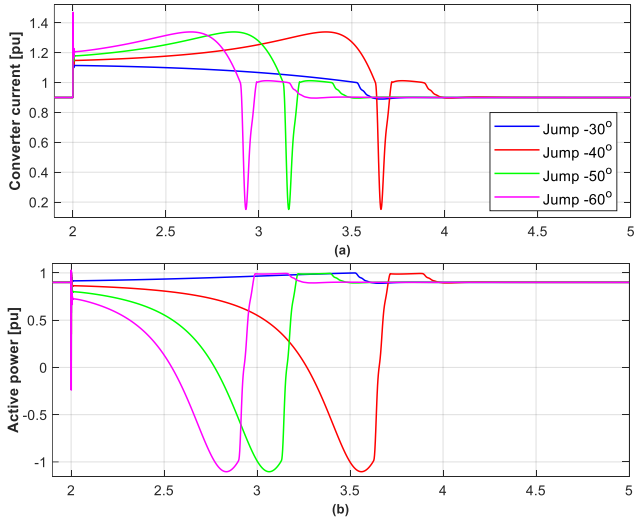

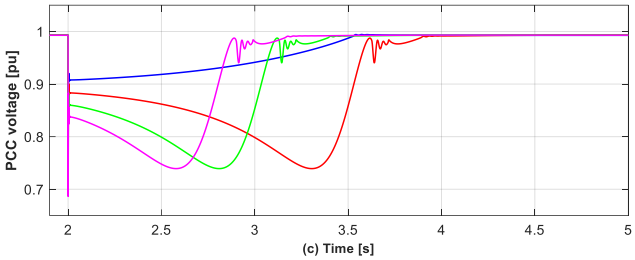

Fig. 8 GFM operation under Case 4 for various phase jumps (a) converter current, (b) active power, and (c) PCC voltage.

4 TVI Re-design based on Voltage Vector Location

Given the limitations of the TVI parameter selection process illustrated in the previous section, the worst case scenario is now modified. Three strategies are then proposed to limit the GFM current, while also maximising utilisation of the GFM capacity. Subsequently, the advantages and disadvantages of the three strategies are discussed.

4.1 TVI Parameter Re-Design Based on Worst Case Scenario

Based on the existing TVI parameter design of (10), it was previously seen that the GFM current is not limited to I_{max} during disturbances, since the maximum voltage across the virtual impedance and output transformer can be larger than V_{ref}. Instead, from Section 3, the worst case scenario aligns with a maximum voltage of $V_{ref} + V_g$ (i.e. $\theta_{vsm} = -\theta_g$). Then condition (10) becomes (12).

$$I_{max} = \frac{V_{ref}+V_g}{\sqrt{\left(R_c+R_g+\tilde{R}_{VI}^{max}\right)^2+\left(X_c+X_g+\tilde{X}_{VI}^{max}\right)^2}}. \quad (12)$$

where $\tilde{R}_{VI}^{max}$ and $\tilde{X}_{VI}^{max}$ are in the same form as (11) and (8). Note that $\sigma_{X/R}^{VI}$ for calculating k_{pR}^{VI} based on (12) should be lower than that based on (10), in order to reduce the oscillatory behaviour of the GFM current [10], as k_{pR}^{VI} obtained by (12) is almost twice that obtained by (10).

In order to demonstrate the effectiveness of (12) for determining the TVI parameters, Cases 5 and 6 are simulated.

Case 5: Same as Case 3, but k_{pR}^{VI} is obtained from (12). For a post-fault impedance, X_g, of 0.02, 0.2 or 0.8 pu, k_{pR}^{VI} is calculated as 2.80, 2.47, 1.36.

Case 6: Same as Case 4, but k_{pR}^{VI} is obtained from (12), with X_g set at 0.2 pu, and k_{pR}^{VI} is calculated as 2.47.

The GFM converter current for Cases 5 and 6 is shown in Figs. 9 and 10. Compared to Figs. 7 and 8, the maximum GFM current for different transmission line impedances and phase jumps is less than 1.2 pu, indicating the effectiveness of the modified TVI parameter design process for limiting the GFM current. However, in comparison to Fig. 7, Fig. 9 shows that during the fault, when X_g is 0.02 and 0.2 pu, the GFM current is ≈1.1 pu, indicating that the converter capacity is not being fully used. Similarly, when comparing Fig. 10 against Fig. 8, the converter is less stable for the -30° phase jump, since the converter current is (overly) constrained by the modified TVI impedance. Hence, (12) should not be directly used when calculating the TVI parameter, k_{pR}^{VI}, and

instead three strategies are now proposed to limit the GFM current while making full use of the converter capacity.

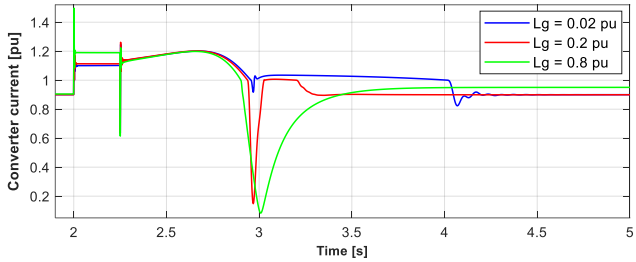

Fig. 9 GFM current with re-designed TVI parameters under Case 5 for different transmission line lengths.

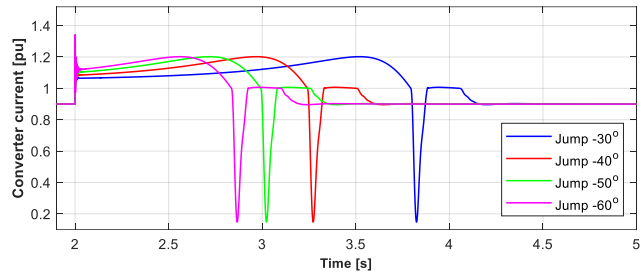

Fig. 10 GFM current with re-designed TVI parameters under Case 6 for different phase jump angles.

4.2 GFM Current Limiting and Capacity Utilisation Strategies

To limit the GFM current and make full use of the converter capacity to support faults and phase jump events, three strategies are proposed.

Strategy 1: The results in Figs. 5 and 8 show that the GFM current is limited for a short fault or small phase jump within 1.2 pu, based on the existing TVI parameter design of (10). Therefore, using the existing TVI parameters, any increase in the GFM internal voltage angle is kept small when clearing a long duration fault or following a large phase jump.

In order to enhance the transient stability of a GFM, a number of methods can be employed, e.g. slowing down the GFM voltage angle increase during the fault (achieved by reducing the droop coefficient [16], freezing the virtual angular speed [17], reducing the active power reference or defining a larger $\sigma_{X/R}^{VI}$ [10]), modifying the existing TVI control structure, or, simply, reserving converter capacity. It should be noted that some transient stability enhancement methods are only suitable for fault events, and not for both fault and phase jump events. Additional simulation results are not presented here to validate Strategy 1, given that the earlier results have shown that the GFM current can be limited within 1.2 pu under the existing TVI parameter design, assuming that the GFM voltage angle is kept small when the fault is cleared or if a phase jump occurs. The obvious downside of Strategy 1 is its inability to ensure that the GFM current is kept within the maximum limit.

Strategy 2: For fault events, switch the TVI parameters from the design based on (10) to that based on (12) when the fault is cleared. Given that such an approach is likely to be problematic in practice, particularly during the switching transient period, additional case studies for Strategy 2 are also not presented here.

Strategy 3: Combining the existing TVI parameter design of (10) with scaling-based current saturation control under conditional integration. The anti-windup integration is shown in Fig. 11, with the current saturation control under anti-windup integration detailed in [18]. The current limit for current saturation control is chosen slightly higher (e.g. 0.05 pu) than that for TVI control, in order that the latter approach mainly limits the converter current, such that the behaviour of a GFM voltage source behind an impedance is retained. However, it follows that Strategy 3 will not use the full GFM current capacity (e.g. 0.05 pu) at its maximum limit.

To demonstrate the current limiting capability of Strategy 3, Cases 6 and 7 are now simulated.

Cases 6 and 7: Same as Case 1 for a 300 ms fault and Case 4 for a -60° grid phase jump, respectively, but TVI is combined with scaling based current saturation control. The maximum current for current saturation control is set at 1.2 pu, leading to 1.15 pu for TVI control ($\sigma_{X/R}^{VI} = 2.5$ and $k_{pR}^{VI} = 1.8$).

The simulation results for Cases 6 and 7 are shown in Fig. 12, and it is seen that the converter current is strictly limited to 1.2 pu (without overshoot) for the two cases, Fig. 12(a). However, the converter current only reaches 1.15 pu during the fault, such that 0.05 pu current capacity is not used. Fig. 12(b) shows that the active power profile is non-smooth, due to the current saturation control activating, which increases analysis complexity.

In conclusion, each strategy has its limitations, such that a proposal is that enhancing GFM transient stability under Strategy 1 should be prioritised, if GFM synchronisation instability still appears, combining with Strategy 2 and/or 3.

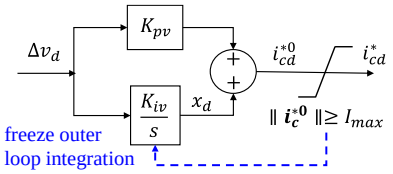

Fig. 11 d-axis current reference generation under scaling-based current saturation control with conditional anti-windup integration for the outer loop voltage PI controller.

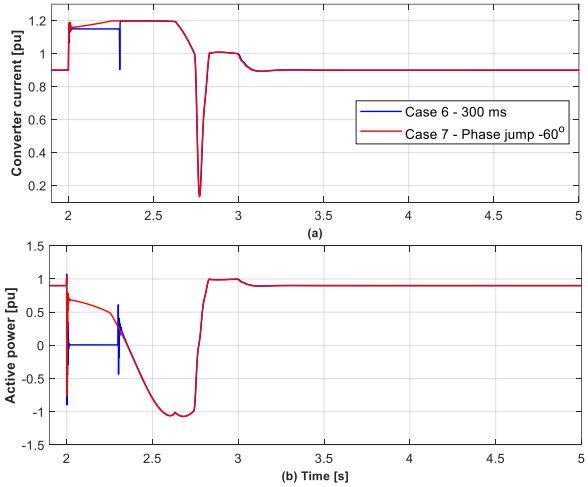

Fig. 12 GFM operation under Cases 6 and 7 (a) converter current, (b) active power.

Table 1 Circuit and control parameters for droop control-based grid-forming converter

Parameters	Value (pu)
R_f, L_f, C_f	0.005, 0.15, 0.066
k_{pv}, k_{iv}, k_{pi}, k_{ii}	0.52, 1.16, 0.74, 1.19
$\sigma_{X/R}^{VI}$	2.5
I_{nom}	1
m_p, m_q	0.02, 0.0001
ω_c, ω_{cq}	31.4 rad/s, 31.4 rad/s

4 Conclusion

Given the current limitations of converters, threshold virtual impedance design aims to restrict the current to a maximum value when a bolted fault is applied at the PCC. However, the converter current limit may actually be exceeded for long duration faults or large grid phase jump events, due to a large angular difference between the GFM internal and PCC voltage vector when a fault is cleared or when a large phase jump occurs, giving rise to a large voltage drop across the virtual impedance and output transformer. Hence, the worst case scenario for calculating TVI parameters is not during a fault, but once the fault is cleared, or when a large grid phase jump occurs. It follows that TVI parameter selection should be based on the GFM internal voltage vector being in anti-phase to the equivalent AC grid, in order to securely limit the GFM current. However, making full use of the GFM current capacity by employing the modified TVI parameter approach is not recommended, and hence three strategies are proposed. A combination of strategies is recommended given their respective limitations.

5 Acknowledgements

The work has been supported by a Ulysses award from the Irish Research Council between UCD and L2EP, ENSAM. It has also been supported by SEAI (Sustainable Energy Authority of Ireland) under RD&D Award 22/RDD/776.

6 References

[1] Hatziargyriou, N., et al.: 'Stability definitions and characterization of dynamic behavior in systems with high penetration of power electronic interfaced technologies', IEEE PES Tech. Rep. PES-TR77 2020.

[2] Rocabert, J., Luna, A., Blaabjerg, F., Rodriguez, P.: 'Control of power converters in AC microgrids', IEEE Trans. Power Electron., 2012, 27, pp. 4734–4749.

[3] Yu, M., et al.: 'Instantaneous penetration level limits of non-synchronous devices in the British power system', IET Renew. Power Gener., 2017, 11(8), pp. 1211-1217.

[4] Zhao, X., Thakurta, P.G., Flynn, D.: 'Grid-forming requirements based on stability assessment for 100% converter-based Irish power system', IET Renew. Power Gener., 2022, 16, pp. 447–458.

[5] Infineon, 'AN2011-05 Industrial IGBT Modules Explanation of Technical Information', November 2015.

[6] Zhao, X., Flynn, D: 'Freezing grid-forming converter virtual angular speed to enhance transient stability under current reference limiting', IEEE 21st Workshop Control Modeling Power Electronics Aalborg, Denmark, 2020.

[7] Bottrell, N., Green, T.C.: 'Comparison of current-limiting strategies during fault ride-through of inverters to prevent latch-up and wind-up', IEEE Trans. Power Electron., 2013, 29, pp. 3786–3797.

[8] Taul, M.G., Wang, X., Davari, P., and Blaabjerg, F.: 'Current limiting control with enhanced dynamics of grid-forming converters during fault conditions', IEEE Trans. Emerg. Sel. Topics Power Electron., 2019, 8(2), pp. 1062-1073.

[9] Paquette, A. and Divan, D.: 'Virtual impedance current limiting for inverters in microgrids with synchronous generators', IEEE Trans. Ind. Appl., 2014, 51(2), pp. 1630-1638.

[10] Taoufik, Q., Wu, H., Wang, X. and Colak, I.: 'Variable virtual impedance-based overcurrent protection for grid-forming inverters: small-signal, large-signal analysis and improvement', IEEE Trans. Smart Grid, 2022, DOI: 10.1109/TSG.2022.3232987

[11] Lu, X., Wang, J., Guerrero, J.M. and Zhao, D.: 'Virtual-impedance-based fault current limiters for inverter dominated AC microgrids', IEEE Trans. Smart Grid, 2016, 9(3), pp. 1599-1612,

[12] Sati, T.E., Azzouz, MA., and Shaaban, M.: 'Optimal protection coordination of islanded microgrids utilizing an adaptive virtual impedance fault current limiter', IEEE Trans. Ind. Appl., 2023, 59(3), pp. 2866-2876.

[13] D'Arco, S., Suul, J.A., Fosso, O.B.: 'Automatic tuning of cascaded controllers for power converters using eigenvalue parametric sensitivities', IEEE Trans. Ind. Appl., 2014, 51, pp. 1743–1753.

[14] Fritzson, P.: Principles of Object-Oriented Modeling and Simulation with Modelica 3.3: A Cyber-Physical Approach, John Wiley & Sons: NJ, USA, 2014.

[15] Qoria, T., et al.: 'Tuning of cascaded controllers for robust grid-forming voltage source converter', Proc. Power Syst. Comput. Conf., 2018.

[16] Qoria, T., et al.: 'Critical clearing time determination and enhancement of grid-forming converters embedding virtual impedance as current limitation algorithm', IEEE Trans. Emerg. Sel. Topics Power Electron., 2019, 8(2), pp. 1050-1061.

[17] Zhao, X. and Flynn, D.: 'Grid-forming converter angular speed freezing to enhance transient stability in 100% grid-forming and mixed power systems', IFAC-PapersOnLine, 2022, 55(9), pp. 425-430.

[18] Zhao, X. and Flynn, D.: 'Stability enhancement strategies for a 100% grid-forming and grid-following converter-based Irish power system', IET Renew. Power Gener., 2022, 16(1), pp. 125-138.